

# Comparative Modelling and Experimental Verification of a PMSM Drive System

Gullu Boztas<sup>1\*</sup> 

<sup>1\*</sup>Firat University, Electrical and Electronics Engineering, Elazig, Turkey. (e-mail: [gboztas@firat.edu.tr](mailto:gboztas@firat.edu.tr)).

## ARTICLE INFO

Received: Apr., 11. 2022

Revised: Jun., 13. 2022

Accepted: Jun, 30. 2022

### Keywords:

Permanent magnet synchronous motor  
Modelling  
Simulation  
Experimental verification

Corresponding author: *Gullu Boztas*

ISSN: 2536-5010 / e-ISSN: 2536-5134

DOI: <https://doi.org/10.36222/ejt.1101838>

## ABSTRACT

This paper presents a comparative study on three simulation models and an experimental model for a Permanent Magnet Synchronous Motor (PMSM) drive system. A realistic modelling and simulation of a PMSM drive system are very useful before developing an experimental study. In particular, analyzing the performance of the motor drive and control algorithm in a simulation environment provides many advantages. The motor and drive system can be tested by using a simulation environment with various realistic scenarios in order to reduce testing costs and time span. Therefore, a comparative simulation study was performed in this paper to show the simulation results similarity with real application results. Three PMSM drive systems were modelled by using MATLAB environment based on SimPowerSystems, Simscape Electrical, and based C-language. All models and experimental system were operated under the same conditions. These models were compared with each other and verified with an experimental system. The waveforms were analyzed comparatively such as current, speed, mechanical position of the motor.

## 1. INTRODUCTION

PMSM is a rotating electric machine having a conventional three-phase stator like that of an induction motor (IM) and permanent magnets mounted on its rotor surface. PMSM is equivalent to an IM in which the air gap magnetic field is generated by a permanent magnet. The stator current of IM contains both magnetizing and torque generating components. It is unnecessary in order to obtain magnetizing current through the PMSM stator for constant air gap flux because the rotor of the PMSM has permanent magnet. The stator current only needs to produce torque. Therefore, the PMSM operates at a higher power factor and PMSM is more efficient due to the absence of magnetizing current according to IM for the same output [1,2]. DC motors used in many applications requiring high performance began to be replaced by PMSMs with the using of magnet materials such as samarium-cobalt (SmCo) and neodymium-ironboron (NdFeB) in the 1970s and 1980s [3]. PMSM has such as high power factor, high power density, robustness, small size, lightness, low noise and high torque compared to other electric motors [4–10]. Permanent magnets are used instead of the field windings in the rotor of the PMSM. Permanent magnets can produce magnetic flux in an air gap without field excitation windings and electrical power losses. PMSM has higher efficiency than other AC motors because the rotor of PMSM produces magnetic flux with permanent magnets. Therefore, PMSM is widely used in

electric vehicle, military and aviation industries [11]. Additionally, PMSMs have become the key and core components of complex electromechanical systems such as robotic application, urban rail vehicles, ship propulsion systems, high-speed elevators and wind power generation because the motors have high efficiency, large torque-inertia ratio, fast dynamic torque response, high overload capacity, wide speed range advantages [12–18]. The phase voltages and currents of the PMSM stator are ideally sinusoidal. The flux of the motor provides an ideal sinusoidal flux distribution by the installation of rotor magnets in the air gap. The installation of the rotor magnets can be in different shapes called as surface mounted, inset radial, interior, and spoke [19]. The location and the shape of the magnets change dynamic features of the motor. DC motor was widely used in position and speed control applications for many years because the motor control is easy. The motor stator currents must be controlled directly in order to obtain the desired performance from PMSMs such as the behavior of DC motors. Accurate speed control of PMSM driver is a complex issue due to the nonlinear relationship between winding current and the rotor speed of the PMSM. Electromagnetically produced torque of the motor is non-linearity due to the magnetic saturation of the rotor core. Therefore, it is difficult in order to control of the motor [20]. AC motor drive systems and motor control schemes have been studied in many literature [21–23]. Field oriented control (FOC) and direct torque control (DTC) are

two control strategies commonly used for industrial motor drives [24]. A comparative study of DTC controlled PMSM is performed using Matlab/Simulink and DSPACE-1104 [25, 26]. A novel method for magnetization fault detection in PMSM is presented by using finite element analysis with simulation environment [27]. FOC is generally the most effective and reliable control method for PMSM drives [28]. Synchronous and asynchronous motors could be controlled just like a DC motor with the introduction of vector control theory in the 1970s. FOC method was first proposed by F. Blaschke in order to control IMs in the early 1970s. The vector control technology has been widely used in high performance AC drives over the past two decades due to the rapid development in power electronics, computing, and microelectronics [29]. The FOC technique provides decoupling of flux and torque similar to that of a DC motor. FOC method includes current control loops in order to control the direct axis current and the quadrature axis current [30, 31]. FOC method commonly used in the control system of the PMSM consists of an internal current loop and an external speed loop. Proportional integral (PI) control is used in speed and current loops in FOC [32].

In this study, 3 different simulation models and experimental results for a PMSM drive system were comparatively analyzed. All simulations were developed in MATLAB environment. Control algorithms and sampling times were the same for all simulations. The first two simulation models were performed using available tools and the other was developed by using the C-language. The details of the blocks used in the simulations were analyzed in detail in the paper. The parameters used in the simulations were taken by measuring from the real system. The simulations and real results were performed under the same conditions. Results were analyzed in terms of motor speed, stator currents and harmonic spectra of the currents. Additionally, the execution times of the simulations were compared for same conditions. This paper is organized as follows: The mathematical model of the PMSM is described in Section 2. The simulation results and experimental verification are presented in Section 3 and Section 4, respectively. Finally, conclusions are discussed in Section 5.

## 2. MATHEMATICAL MODELLING OF PMSM

The  $d$  and  $q$ - axis currents converted from 3 to 2 phases in an AC motor represent the field and armature current, respectively. The control of AC machine can be achieved with different algorithms by using static and rotating reference frames. The coordinate system is generally obtained by the Clarke Transform of the  $\alpha\beta$ -fixed reference frame and the Park Transform of the  $dq$ -rotating reference frame. The equivalent circuit of the PMSM is illustrated in Fig. 1. In this study, rotating frame was aligned with the phase A axis. Therefore, the voltage equations can be derived as given in the Eq. (1).  $c$  refers to cosine and  $s$  refers to sinus function in the equation.

$$\begin{bmatrix} u_d \\ u_q \\ u_0 \end{bmatrix} = \frac{2}{3} \begin{bmatrix} c(\omega t) & c(\omega t - 2\pi/3) & c(\omega t + 2\pi/3) \\ s(\omega t) & s(\omega t - 2\pi/3) & s(\omega t + 2\pi/3) \\ 1/2 & 1/2 & 1/2 \end{bmatrix} \begin{bmatrix} u_a \\ u_b \\ u_c \end{bmatrix} \quad (1)$$

where  $u_a$ ,  $u_b$  and  $u_c$  are the three phase voltages of the stator windings fed by inverter output. The voltage equations of the PMSM can be derived as shown in Eq. (2) and Eq. (3). Additionally, linkage fluxes of the  $dq$ -axis are given in Eq. (4) and Eq. (5).

$$u_d(t) = R_s i_d(t) + \frac{d}{dt}(L_d i_d(t)) - \omega_e L_q i_q(t) \quad (2)$$

$$u_q(t) = R_s i_q(t) + \frac{d}{dt}(L_q i_q(t)) + \omega_e L_d i_d(t) + \omega_e \psi_m \quad (3)$$

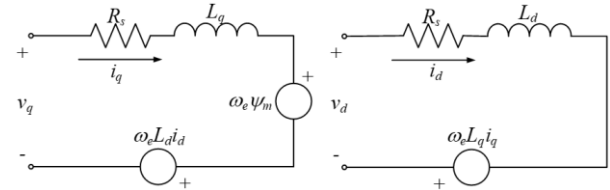


Figure 1. Equivalent circuit of the PMSM

$$\psi_d = \psi_m + L_d i_d \quad (4)$$

$$\psi_q = L_q i_q \quad (5)$$

where,  $i_d$  and  $i_q$  are  $dq$ -axis current.  $\omega_e$  is the electrical velocity of the PMSM. Additionally,  $\psi_d$  and  $\psi_q$  are  $dq$ -axis linkage fluxes while  $\psi_m$  is the magnet flux of the rotor.  $R_s$ ,  $L_d$  and  $L_q$  are stator winding resistance,  $dq$ -axis stator inductance, respectively. These inductances represent the relation between phase inductance and the position of rotor due to the rotor saliency. The measured inductance between the  $a$  and  $b$  phases is given in Eq. (6).

$$L_{ab} = L_d + L_q + (L_d - L_q) \cos(2\theta_e + \pi/3) \quad (6)$$

where  $\theta_e$  is electrical angle of the PMSM rotor. The mechanical equations of the PMSM are given as shown in Eq. (7) and Eq. (8).

$$T_e = T_L + J \frac{d\omega_m}{dt} + B\omega_m \quad (7)$$

$$T_e = \frac{3}{2} p (\psi_m i_q + (L_d - L_q) i_d i_q) \quad (8)$$

where  $T_e$  and  $T_L$  represent the electromagnetic torque and load torque, respectively.  $J$  and  $B$  are the moment of inertia and the friction.  $\omega_m$  is the mechanic velocity of the PMSM and  $p$  is pole pair of the motor.

Vector control algorithm and PMSM's model require Park and Inverse-Park transformation. The transformation equations can be derived by using vector diagram of the  $abc$ -frame which is give in Fig. 2. Park transformation uses the three phase vectors to transform  $dq$  rotating frame. The equations of Park transformations are given in Eq. (9) - Eq. (11). The inverse Park transformation is used to derive  $abc$ -frame vectors which are given in Eq. (12) - Eq. (14). The rotating frame alignment to 90 degrees when  $\omega t$  is zero.

$$V_d = \frac{2}{3} (V_a \sin(\omega t) + V_b \sin(\omega t - \frac{2\pi}{3}) + V_c \sin(\omega t + \frac{2\pi}{3})) \quad (9)$$

$$V_q = \frac{2}{3} (V_a \cos(\omega t) + V_b \cos(\omega t - \frac{2\pi}{3}) + V_c \cos(\omega t + \frac{2\pi}{3})) \quad (10)$$

$$V_0 = \frac{1}{3} (V_a + V_b + V_c) \quad (11)$$

$$V_a = V_d \sin(\omega t) + V_q \cos(\omega t) + V_0 \quad (12)$$

$$V_b = V_d \sin\left(\omega t - \frac{2\pi}{3}\right) + V_q \cos\left(\omega t - \frac{2\pi}{3}\right) + V_0 \quad (13)$$

$$V_c = V_d \sin\left(\omega t + \frac{2\pi}{3}\right) + V_q \cos\left(\omega t + \frac{2\pi}{3}\right) + V_0 \quad (14)$$

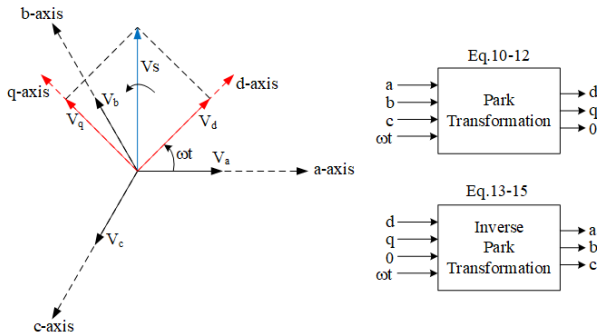


Figure 2. abc-frame and dq-frame for Park transformation

### 3. SIMULATION OF PMSM DRIVE SYSTEM

In this study, PMSM models were obtained by using MATLAB environment. Three different models were created separately and tested under the same conditions. All simulation models were operated with  $1.6 \mu\text{s}$  sample time. The same control blocks, labeled as Field Oriented Control (FOC) and switching technique Space Vector Pulse Width Modulation (SVPWM) shown in Fig. 3, were used in all simulations. The internal block diagrams of control and SVPWM with dead-time ( $3.2 \mu\text{s}$ ) are given in Fig. 3(b). The parameters of the PI controllers are determined using Internal Model Control technique [33]. The PI parameters of speed controller were determined as  $k_p(\text{speed}) = 0.156$  and  $k_i(\text{speed}) = 13.431$ . The PI controller parameters of the  $dq$ -axis were determined as  $k_p(dq) = 21.671$  and  $k_i(dq) = 29,759.12$ . A switching frequency of 16 kHz, which is also used in the experimental system, was selected in the simulation. Three simulation environments are named as SimPowerSystems, Simscape Electrical, and C-language model.

MATLAB has some tools for modelling/simulating electrical power systems included power electronics and electric machines. One of these is SimPowerSystems which is named as Specialized Power Systems for new version of MATLAB. It can be easily connected commonly used Simulink blocks as shown in Fig. 4(a). Many applications of power systems, electrical machines and power electronics can be carried out easily by using this tool. Especially, it helps to develop control algorithms for motor drive applications of any kind of motor type. In this study, the PMSM model and its driver system were used as shown in the Fig. 4(a). A single-phase voltage source was used 220 V, 50 Hz and the source rectifiers by using a full-wave rectifier based on diode. The diode parameters have the same values as the diode KBPC3510 in the experimental system. The inverter block is used with parameters that same values as a PM20CSJ-060 coded IGBT inverter module. The back electromotive force waveform was selected as sinusoidal in the PMSM block configuration because the motor type is a surface mounted PMSM in the experimental study. The DC-link capacitor value was taken as  $3 \times 470 \mu\text{F}$  which has been selected in the real application. Simscape Electrical toolbox is a new generation simulation environment for modelling and simulating electronic, electrical power systems, and electric machines like

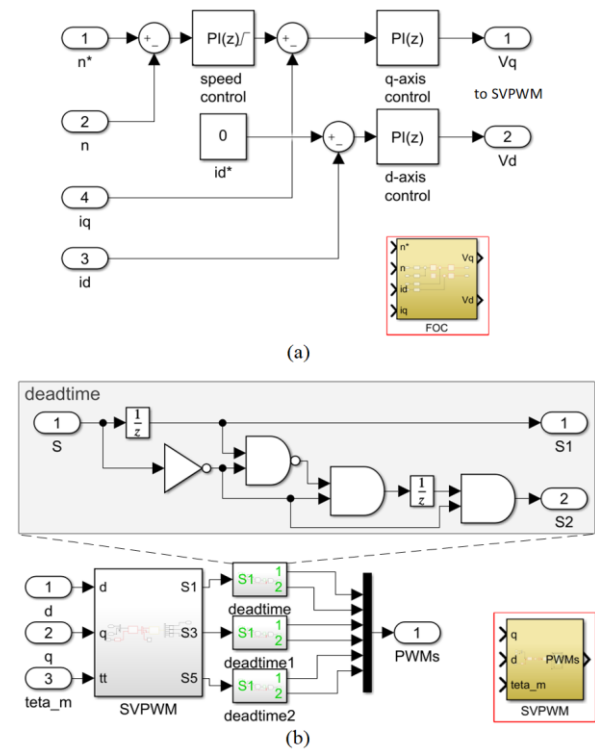


Figure 3. a) Block diagram of control, and b) SVPWM and dead-time blocks

SimPowerSystems. Additionally, Simscape Electrical toolbox is also integrated mechanical, hydraulic, thermal, and other physical systems. SPICE models are also supported by this tool. In this study, existent power electronics devices are used in the simulation environment as shown in Fig. 4(b). The diodes can be configured differently, such as exponential or piecewise linear. In this simulation, the diode and IGBT parameters, all electrical and mechanical values are used the same as in the previous mentioned simulation. Additionally, all mechanical variables can be connected externally as shown in the Fig. 4(b) without the need to use a mechanical variable in the motor model. Thus, a desired mechanical model can be connected to the motor by using Simscape Driveline blocks as a load. A local solver configuration was used in the simulation with backward Euler solver type. MATLAB supports free and open source software development environment Mingw-w64 C-language. In this study, simplified PMSM was developed by using Mingw-w64 C with mathematical equations mentioned first section of this paper. The model masked with a subsystem as shown in Fig. 4(c). The motor winding ports fed from inverter voltage outputs are labeled as “U, V, W”. The “ $T_m$ ” port is the input mechanical torque of the load. Signal routing labeled “Load” is used for load output in all simulations.

The inverter block only converts PWM signals to the voltage signal using by multiplying half of the dc-link voltage value with the difference between the upper and lower switches’ states. The losses of the semiconductor switches were ignored in the inverter block. The interior block diagram of PMSM model based on script is shown in Fig. 5a. The detailed script is given in Fig. 5b. The variables in red are pointers that represent input and output of the PMSM block. The electrical and mechanical equations were defined in the second section of the paper. The coulomb and viscous friction model was added as labeled “cvf” in the script. The motor was not operated at negative speed region. In this study, a simplified model was compared with other models and a real system. Therefore, many system losses were neglected except for the simplified equations. The model presented in Fig. 5 can

be obtained easily in any simulation environment. The simulation models were compared with each other as shown in Fig. 6. The motor was operated at a nominal constant speed of 3000 rpm at half-load and full-load transition. The PMSM was started under the half-load condition and the motor was operated for full-load after 1.5 seconds. The full-load transition is given in detailed Fig. 6b and Fig. 6d for speeds and stator currents, respectively. Subsequently, load was reduced in half of rated load. The transition details are shown in Fig. 6c and Fig. 6e. It is possible to say that all the simulation models give results very close to each other. The harmonic contents of the currents were different although the results were similar. The Total Harmonic Spectrum (THD) at the full-load condition was calculated as 2.3%, 3.89%, 2.04% for Simpower model, Simscape model and C-model, respectively. Additionally, the execution times of the simulations were different from each other. The simulations were performed on a computer with a clock frequency of 4.2 GHz. For 1 second simulation time with  $1.6 \mu\text{s}$  sampling time, execution times are required 20 seconds, 83 seconds, 13 seconds for Simpower model, Simscape model and C-model, respectively. A large amount of execution time was required for Simscape model.

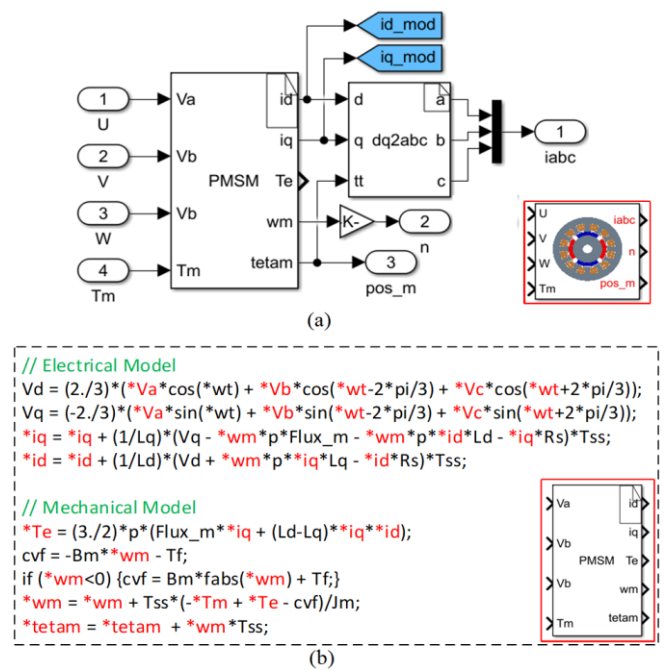


Figure 5. a) Interior block diagram of script based PMSM model, b) Script based model

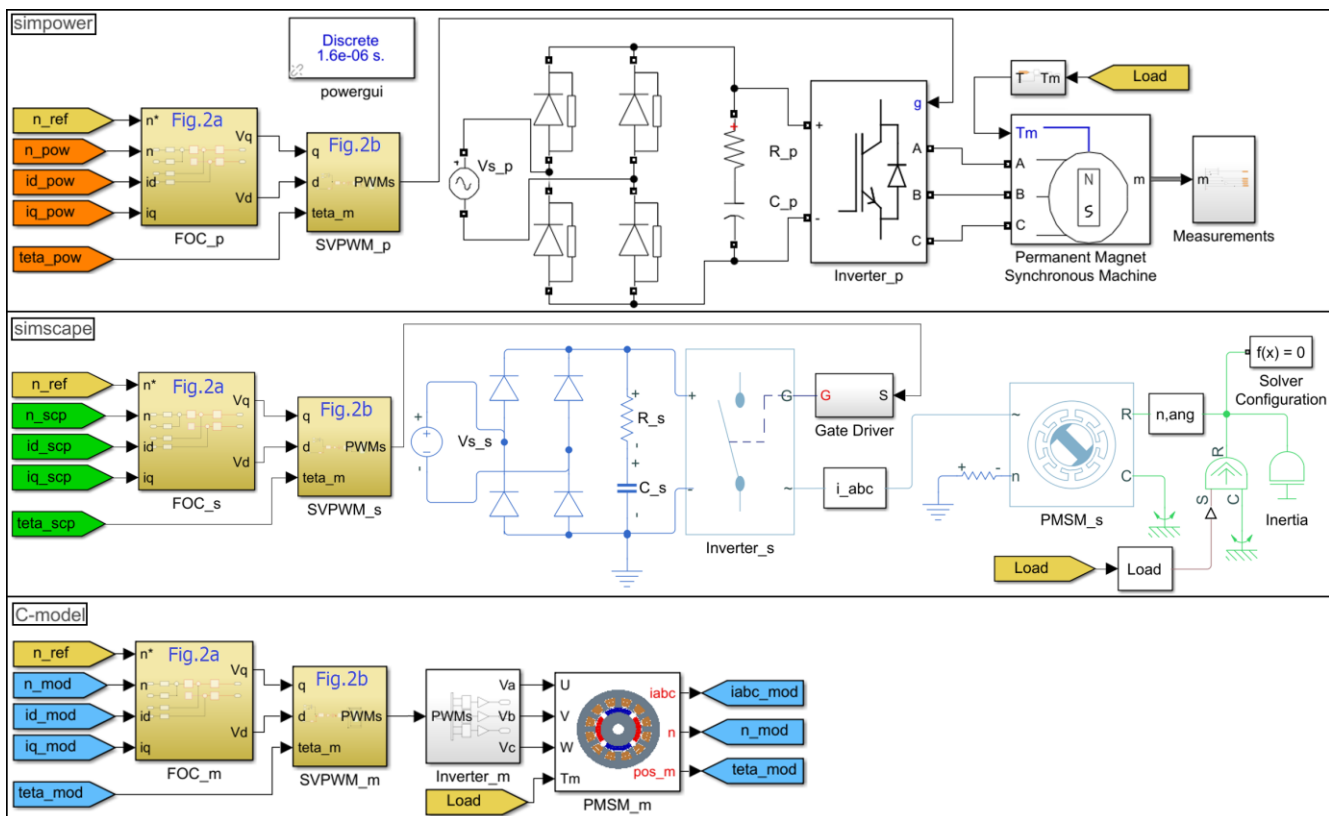


Figure 4. Simulation diagram of PMSM control based on; a) SimPowerSystems, b) Simscape Electrical, c) C-language model

#### 4. EXPERIMENTAL VERIFICATION

The models were compared with a real system shown in Fig. 7 after the mentioned models were compared among themselves. All parameters used in the simulation environment are the values measured from the real system. A surface-mount PMSM was used for this application. The motor parameters are given in Table I. The motor has a 10,000 pulse/rev resolution encoder which is connected to the inverter and 12-bit Digital Analog Converter (DAC). The speed and mechanical position were measured by a scope connected to the DAC. The stator current was measured via a clamp sensor

connected to scope. A magnetic-powder brake was used as a load as shown in the Fig. 7. The PMSM was operated for 12 seconds as shown in Fig. 8. The B-channel in the scope shows motor speed in 1,000 rpm/V scale. The D-channel of the scope measures the U-phase stator winding current of the PMSM. The motor was operated at half-load condition for about 5 seconds as shown in the current waveform. The PMSM was then operated at full-load for about 4 seconds. The time-base was set as 1 sec/div in the scope. The channel of current probe was set to 2 A/div as shown in the Fig. 8a. The effective current of half-load and full-load are measured about 0.84 A and 1.63 A, respectively. Similar results were performed in

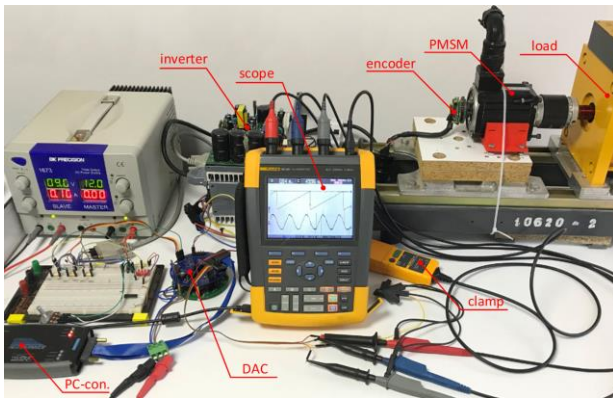


Figure 7. Experimental setup

TABLE I  
PARAMETERS OF THE MOTOR

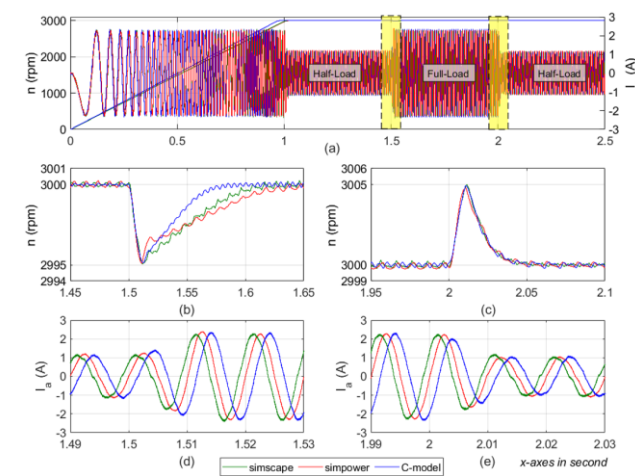


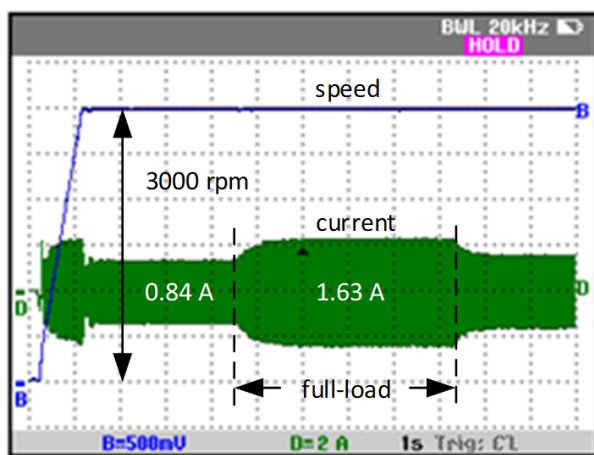
Figure 6. a) Speed and stator current, b,d) Full-Load transition, c,e) Half-Load transition.

Motor parameter	Value
Armature resistance ( $R_s$ )	7.514 $\Omega$
d-axis inductance ( $L_d$ )	15.78 mH
q-axis inductance ( $L_q$ )	15.78 mH
Pole number (P)	4
Rotor Moment of Inertia ( $J_m$ )	1.0314*10 <sup>-3</sup> kg*m <sup>2</sup>
Friction factor ( $B_m$ )	8.2*10 <sup>-6</sup> N*m*s

the simulation environment as shown in the Fig. 8b. Current response at load transitions is not similar to that in the simulation environment due to the magnetic powder brake dynamics coupled to the motor as a load. The load used in the experimental study cannot perform an instantaneous output torque transition. The load can reach the set value after a short latency as shown in the experimental results. This nonlinear behavior is entirely due to the dynamics of magnetic powders in the load system. For this reason, there was no need to model the load dynamics in the simulation environment.

The signals given in Fig. 8 were analyzed in detailed for both simulation and experiment environment as shown in Fig. 9 for under full-load and half-load conditions. Fig. 9a and Fig. 9b present the experimental results. The B-channel in blue is the PMSM speed, C-channel in black is mechanical position and D-channel in green is the stator current of the motor in the Fig. 9a and Fig. 9b. Similarly, the simulation results are presented in Fig. 9c and Fig. 9d for different load conditions. Due to the 4 poles of motor, two periods of a current waveform are seen versus one period of a mechanical position of the motor. The electrical frequency is twice the mechanical frequency. For this reason, the mechanical frequency is 50 Hz while the motor is rotating at 3000 rpm as shown in the Fig. 10a and Fig. 10b. The reason why the simulation results do not appear in the same time axis is that the PMSM models cannot reach the speed set at the same time.

Fast Fourier transform (FFT) analysis was performed for the obtained results at the full-load condition as given in Fig. 10. Percentage values are used according to the magnitude value of the fundamental signals which are labeled as yellow in the figure. The bars in spectra at the same frequencies are shown in similar colors to make it easier to understand. Simscape result was obtained as 3.85% as the closest value to the experimental result while the real system current THD simulation environment. was calculated as 4.17%. The current THD of the Simpower and script based models are obtained as 1.8% and 2.02%, respectively. As a result of the FFT analysis, it is possible to say that the simulation performed with Simscape gives a more realistic result. It is possible to say that the THD values and spectrum amplitudes obtained in the experimental and Simscape simulation results are similar to each other. Brief comparisons of the models are given in Table II.



B:1000rpm/V, D:2A/div, Time-base:1sec/div

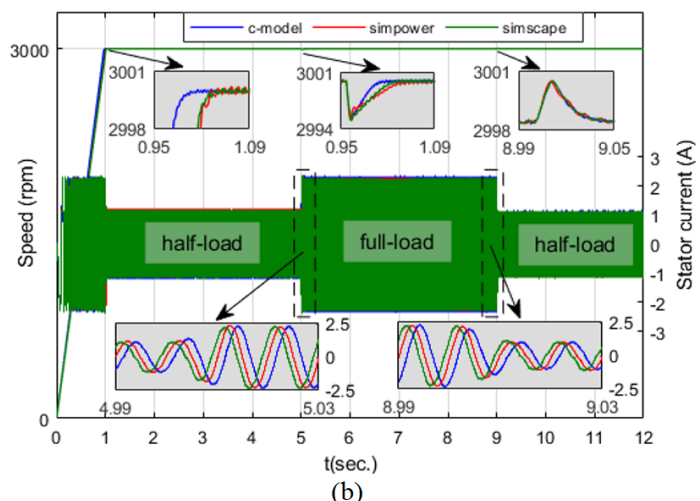


Figure 8. Speed and stator current; a) Experimental results b) Simulation results

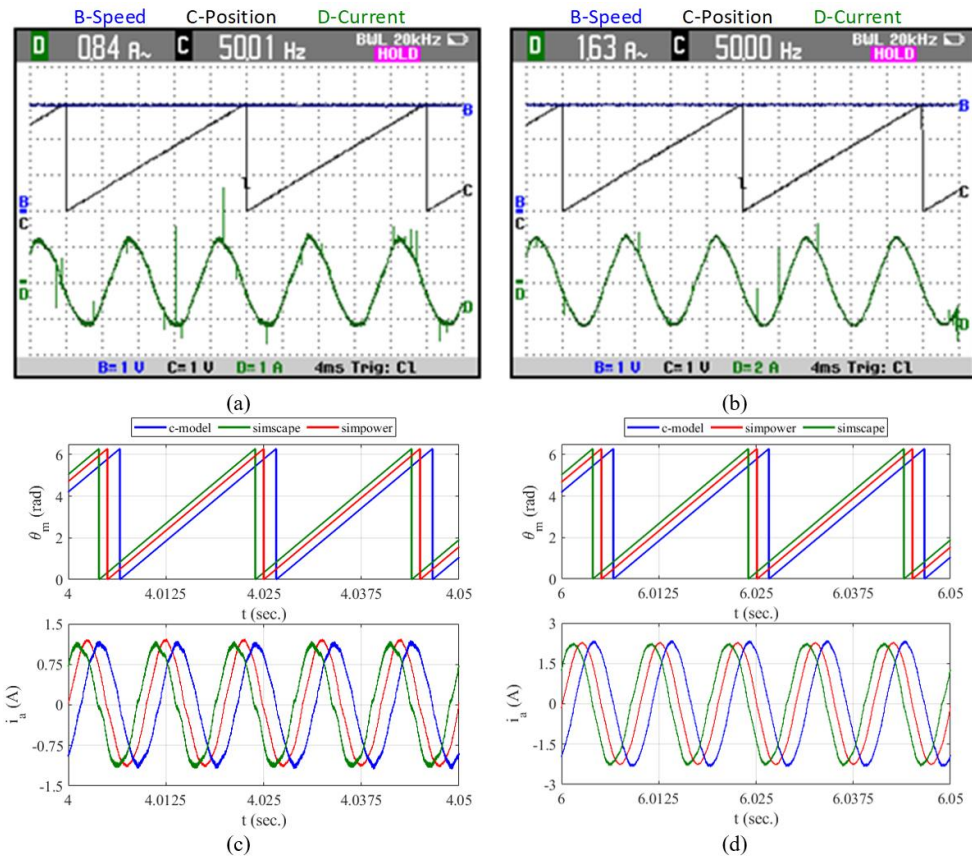


Figure 9. Experimental; a) half-load, b) full-load, Simulation; c) half-load, d) full-load

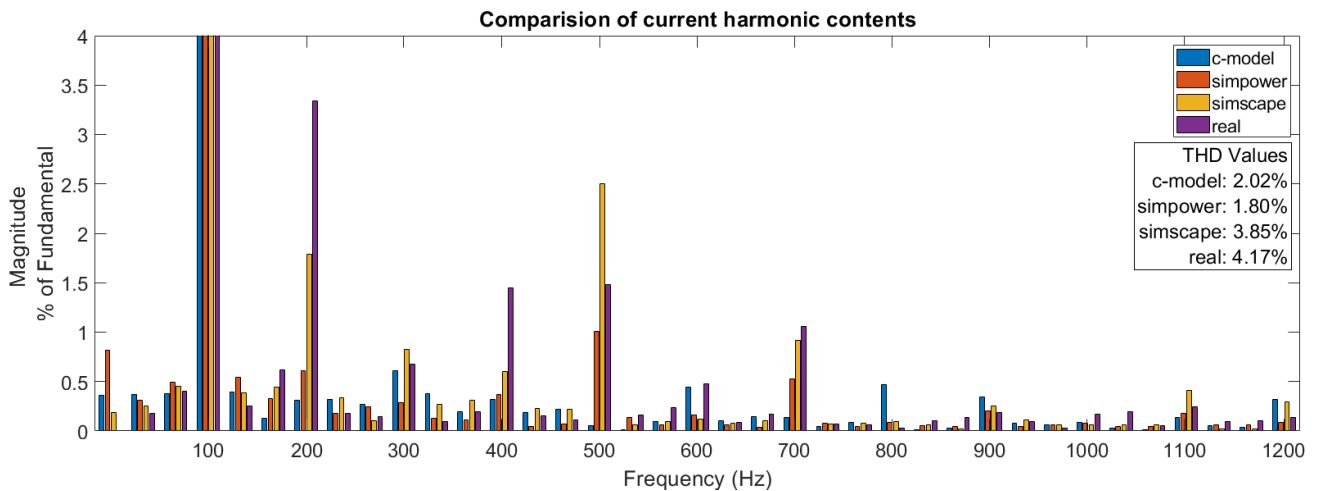


Figure 10. FFT spectra of the stator current at full-load

TABLE II

BRIEF OF COMPARISON OF MODELS

	Simpower	Simscape	C-language	Real system
Execution time	20 sec.	83 sec.	13 sec.	1 sec.
Current $i_a$ THD	1.80 %	3.85 %	2.02 %	4.17 %
Spend time	Medium	Medium	Low	High
Platform support	MATLAB	MATLAB	Many	Real

### 5. CONCLUSION

The interest in PMSM is increasing in many application areas, especially in robotics, automation, and military. Therefore, working with a simulation environment is much easier and cost-effective than working on a real system environment. For this reason, obtaining a realistic simulation result is an important issue. The simulation environment

offers various conditions for developing a real system before it can be experimentally performed. Simulation work is particularly advantageous for developing algorithms and software in motor drive applications. Nowadays, there are many simulation platforms which offer user friendly tool. Among these platforms, MATLAB software, which is widely preferred from the academic community and some commercial companies, was used in this paper. The PMSM drive systems obtained by using Simpower, Simscape, and C-language were compared with each other. However, comparing the simulations among themselves does not give an idea of which one is more realistic. Therefore, all these simulation results were compared with a real system. It is possible to say that all simulations give similar results when all the results are compared to the experimental results. The C-language based PMSM model was obtained with a very low execution time. More accurate results were achieved by using

Simscape model. It can be said that the sample time and real system parameters affected the results. In addition, it was presented that the addition of inverter switching dead-time is a critical issue in a motor drive circuit to obtain more realistic results from the simulation environment. However, it should be said that the simulation results need a longer execution time to obtain a more realistic result.

## REFERENCES

- [1] P. Pillay, and R. Krishnan, "Modeling, Simulation, and Analysis of Permanent-Magnet Motor Drives. Part I: The Permanent Magnet Synchronous Motor Drive," IEEE Transactions on Industry Applications, vol.25, no.2, pp.265–273, 1989.
- [2] O. Aydogmus, and S. Sunter, "Implementation of ekf based sensorless drive system using vector controlled pmsm fed by a matrix converter," International Journal of Electrical Power & Energy Systems, vol. 43, no. 1, pp. 736–743, 2012.
- [3] A. Kumar, S. Marwaha, A. Singh, and A. Marwaha, "Performance investigation of a permanent magnet generator. Simulation Modelling Practice and Theory," vol. 17, no. 10, pp. 1548–1554, Nov 2009.
- [4] W. Wang, Y. Feng, Y. Shi, M. Cheng, W. Hua, and Z. Wang, "Direct Thrust Force Control of Primary Permanent-Magnet Linear Motors with Single DC-Link Current Sensor for Subway Applications," IEEE Transactions on Power Electronics, vol. 35, no. 2, pp. 1365–1376, Feb. 2020.
- [5] M. Cheng, W. Hua, J. Zhang, and W. Zhao, "Overview of stator-permanent magnet brushless machines," IEEE Transactions on Electronics, vol. 58, no. 11, pp. 5087–5101, Nov 2011.
- [6] G. Huang, E. F. Fukushima, J. She, C. Zhang, and J. He, "Estimation of sensor faults and unknown disturbance in current measurement circuits for pmsm drive system," Measurement, vol. 137, pp. 580–587, 2019.
- [7] W. Wang, Z. Lu, W. Hua, Z. Wang, and M. Cheng, "A Hybrid Dual-Mode Control for Permanent-Magnet Synchronous Motor Drives," IEEE Access, vol. 8, pp. 105864–105873, 2020.
- [8] W. Tong, S. Dai, S. Wu, and R. Tang, "Performance comparison between an amorphous metal pmsm and a silicon steel pmsm," IEEE Transactions on Magnetics, vol. 55, no. 6, Jun 2019.
- [9] X. Yuan, Sh. Zhang, and C. Zhang, "Enhanced robust deadbeat predictive current control for PMSM drives," IEEE Access, vol. 7, pp. 148218–148230, 2019.
- [10] F. Grouz, L. Sbita, M. Boussak, and A. Khlaief, "FDI based on an adaptive observer for current and speed sensors of PMSM drives," Simulation Modelling Practice and Theory, vol. 35, pp. 34–49, Jun 2013.
- [11] D. W. Seo, Y. Bak, S. Cho, K. Bae, and K. B. Lee, "An improved flying restart method of sensorless PMSM drive systems fed by an ANPC inverter using repetitive zero voltage vectors," 2019 IEEE Applied Power Electronics Conference and Exposition (APEC), 17-21 March, 2019.
- [12] S. Morimoto, Y. Tong, and T. Hirasu, "Loss Minimization Control of Permanent Magnet Synchronous Motor Drives," IEEE Transactions on Industrial Electronics, vol. 41, no. 5, pp. 511–517, 1994.
- [13] T.M. Jahns, G. B. Kliman, and T. W. Neumann, "Interior Permanent-Magnet Synchronous Motors for Adjustable-Speed Drives," IEEE Transactions on Industry Applications, vol. IA-22, no. 4, pp. 738–47, 1986.
- [14] Z. Chen, M. Tomita, S. Doki, and S. Okuma, "An extended electromotive force model for sensorless control of interior permanent-magnet synchronous motors," IEEE Transactions on Industrial Electronics, vol. 50, no. 2, pp.288–295, Apr. 2003.
- [15] S. Morimoto, Y. Takeda, and T. Hirasu, "Current Phase Control Methods for Permanent Magnet Synchronous Motors," IEEE Transactions on Power Electronics, vol. 5, no. 2, pp. 133–139, 1990.
- [16] X. Chen, J. Hu, K. Chen, and Z. Peng, "Modeling of electromagnetic torque considering saturation and magnetic field harmonics in permanent magnet synchronous motor for HEV," Simulation Modelling Practice and Theory, vol. 66, pp. 212–225, Aug. 2016.
- [17] W. Liu, L. Liu, Il Yop Chung, D. A. Cartes, and W. Zhang, "Modeling and detecting the stator winding fault of permanent magnet synchronous motors," Simulation Modelling Practice and Theory, vol. 27, pp. 1–16, Sep. 2012.
- [18] S. Maiti, C. Chakraborty, and S. Sengupta, "Simulation studies on model reference adaptive controller based speed estimation technique for the vector controlled permanent magnet synchronous motor drive," Simulation Modelling Practice and Theory, vol. 17, no. 4, pp. 585–596, Apr. 2009.
- [19] G. Boztas, and O. Aydogmus, "Comparison of Permanent-Magnet Assisted Synchronous Reluctance Motors with Different Rotor Structures," 11th International Conference on Electrical and Electronics Engineering (ELECO), 28-30 November, 2019.
- [20] F. Dalvand, M. Mardaneh, and J. Milimonfared, "Development of genetic-pi based controller for interior permanent magnet synchronous motor drive over wide speed range," 3rd IET International Conference on Power Electronics, Machines and Drives - PEMD 2006, 4-6 April, 2006.
- [21] T. M. Jahns, "Flux-weakening regime operation of an interior permanent-magnet synchronous motor drive," IEEE Transactions on Industry Applications, vol. IA-23, no. 4, pp. 681–689, 1987.
- [22] M. Miyamasu and K. Akatsu, "An approach to generate high reluctance torque in an inset-type PMSM by square current excitation," 2012 IEEE International Conference on Power and Energy (PECon), 2-5 December, 2012.
- [23] T. Ameid, A. Menacer, H. Talhaoui, and I. Harzelli, "Rotor resistance estimation using extended kalman filter and spectral analysis for rotor bar fault diagnosis of sensorless vector control induction motor," Measurement, vol. 111, pp. 243–259, 2017.
- [24] A. Gundogdu, R. Celikel, B. Dandil, and F. Ata, "Fpga in-the-loop implementation of direct torque control for induction motor," Automatika, vol. 62, no. 2, pp. 275–283, 2021.
- [25] A. Ghamri, R. Boumaaraf, M.T. Benchouia, H. Mesloub, A. Goléa, and N. Goléa, "Comparative study of ann dtc and conventional dtc controlled pmsm motor," Mathematics and Computers in Simulation, vol. 167, pp. 219–230, 2020.
- [26] H. Mesloub, R. Boumaaraf, M.T. Benchouia, A. Goléa, N. Goléa, and K. Srairi. Comparative study of conventional dtc and dtc svm based control of pmsm motor — simulation and experimental results. Mathematics and Computers in Simulation, vol. 167, pp. 296–307, 2020.
- [27] J. Zhang, A. Tounzi, A. Benabou, and Y. L. Menach, "Detection of magnetization loss in a pmsm with hilbert huang transform applied to non-invasive search coil voltage," Mathematics and Computers in Simulation, vol. 184, pp. 184–195, 2021.
- [28] K. Gulez, A. A. Adam, I. E. Buzcu, and H. Pastaci, "Using passive filters to minimize torque pulsations and noises in surface PMSM derived field oriented control," Simulation Modelling Practice and Theory, vol. 15, no. 8, pp. 989–1001, Sep. 2007.
- [29] M. Marufuzzaman, M. B. I. Reaz, and M. A. M. Ali, "FPGA implementation of an intelligent current dq PI controller for FOC PMSM drive," 2010 International Conference on Computer Applications and Industrial Electronics, 5-8 December, 2010.
- [30] W. Wang, Y. Feng, Y. Shi, M. Cheng, W. Hua, and Z. Wang, "Fault-Tolerant Control of Primary Permanent-Magnet Linear Motors with Single Phase Current Sensor for Subway Applications," IEEE Transactions on Power Electronics, vol. 34, no. 11, pp. 10546–10556, Nov. 2019.
- [31] S. G. Petkar and T. V. Kumar, "Computationally efficient model predictive control of three-level open-end winding permanent-magnet synchronous motor drive," IET Electric Power Applications, vol. 14, no. 7, pp. 1210–1220, Jul. 2020.
- [32] X. Liu, H. Yu, J. Yu, and L. Zhao, "Combined Speed and Current Terminal Sliding Mode Control with Nonlinear Disturbance Observer for PMSM Drive," IEEE Access, vol. 6, pp. 29594–29601, May 2018.
- [33] O. Wallmark, "Control of a Permanent Magnet Synchronous Motor with Non-Sinusoidal Flux Density Distribution," PhD thesis, Chalmers University of Technology, Goteborg, Sweden, 2001.

## BIOGRAPHIES

**Gullu Boztas** received the B.S. (2011), M.S. (2015), and Ph.D. (2019) degree in electric-electronics engineering from the University of Firat Since 2013, she has been a Research Assistant in Department of Electrical & Electronics Engineering, Faculty of Technology, Firat University, Elazig, Turkey. Her interests include power electronics and electric machines..